Dendron-Stabilized Liquid Crystalline Blue Phases with an Enlarged Controllable Range of the Photonic Band for Tunable Photonic Devices

*Seishi Shibayama, Hiroki Higuchi, Yasushi Okumura, and Hirotsugu Kikuchi**

Liquid crystalline blue phases (BPs) show excellent potential for application in tunable photonic devices because they possess the unique optical property that the selective 3D Bragg diffraction in a visible wavelength region can be continuously shifted using an electric field. A new approach to simultaneously extend the wavelength range of field-induced Bragg diffraction shift and the temperature range of thermodynamically stable BPs is critically needed. Here, a new BP material system is shown using a dendron molecule to extend simultaneously the two BP ranges. One is the temperature range of thermodynamically stable BPs, which is expanded from 2.1 to 4.6 °C. The other is the reversible maximum shift range of Bragg wavelength on the electric field, which is extended from 85 to 109 nm. The physical mechanism of the dendron-stabilizing effect in BPs is discussed in terms of elastic property and orientational order of liquid crystal molecules.

1. Introduction

Photonic crystals attract substantial interest due to their tremendous potential for advanced applications to photonic devices.[1–3] In particular, tunable photonic crystal offers the advantage of being able to control the bandgap via external stimuli and is applicable to highly sophisticated optical devices. Liquid crystalline blue phases (BPs) are one of the candidates for tunable photonic crystals, possessing an optical stopband in the visible wavelength range due to their lattice periods of several hundred nm, which can be continuously shifted by electric fields.[4–7] Though originally BPs appeared over a very narrow temperature range (typically about 1 °C) between isotropic phase (Iso) and chiral nematic phase (N*), polymer-stabilized blue phases (PSBPs) have been found to show a large temperature range of stable BPs of more than 60 °C; they also show excellent performance for application to liquid crystal displays, including fast electro-optical responses of less than 1 ms (conventional nematic phase shows several ms in response time) and a large Kerr constant.[8–24] Also, BPs show a great benefit compared to N*, which shows a 1D stopband as a photonic crystal,[25,26] because the lasing threshold energy needed to excite the BPs is much lower than that of N*.[27–29] Furthermore, BPs have 3D giant lattices, which can lead to a full bandgap photonic crystal if the refraction indices are sufficiently different between the disclination cores and the double-twist cylinders.[30–32] However, the tunability of the bandgap in BPs is almost lost in PSBPs because the continuous shifts of the stopbands by the electric field hardly occur due to the fixed lattice of polymer networks formed along the disclination lines.[9] Recently, materials showing a wide temperature range of BPs without polymer have been actively studied.[30,33–46] However, most materials reported so far show a wide temperature range of BPs on cooling process, but still have a narrow range on heating. From a viewpoint of practical applications, the long-term stability of BPs is required. Generally, thermodynamic equilibrium phase-transition points are reflected on a heating process rather than a cooling process, because a supercooling easily occurs on cooling. Therefore, it is a remaining challenge to achieve two targets simultaneously: i) a wide temperature range of BPs appears in both heating and cooling processes and ii) stopbands of BPs that can be controlled by an external field.

Here we present a new material system using a dendron molecule (**Figure 1**), which shows relatively enlarged temperature ranges on heating and cooling, as well as an electric field-induced reversible shift of stopbands in BPs. The thermodynamic stability of BPs in the new material system is discussed from the viewpoint of free energies and the stability with respect to the electric force.

2. Results and Discussion

2.1. Temperature Range of Thermodynamically Stable Liquid Crystalline Blue Phases

In general, BPs are easily supercooled at BPs-N* transition on cooling. Therefore we must be careful not to misunderstand

S. Shibayama
Department of Applied Science for Electronics and Materials
Kyushu University
6-1 Kasuga-koen, Kasuga, Fukuoka 816-8580, Japan
Dr. H. Higuchi, Prof. Y. Okumura, Prof. H. Kikuchi
Institute for Material Chemistry and Engineering
Kyushu University
6-1 Kasuga-koen, Kasuga, Fukuoka 816-8580, Japan
E-mail: kikuchi@cm.kyushu-u.ac.jp

DOI: 10.1002/adfm.201202497

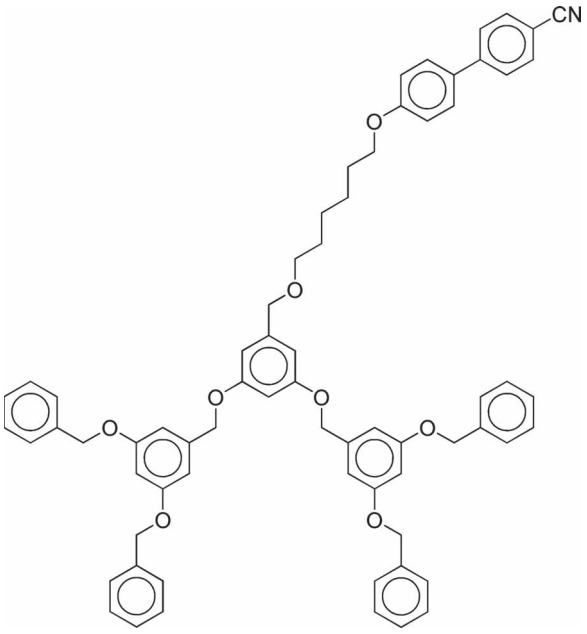

Figure 1. Chemical structure of the dendron molecule.

the BPs' stable temperature range. In this study, the temperature ranges of thermodynamically stable BPs were carefully determined by four steps as follows: i) the phase-transition temperatures and the kinds of phase were measured with polarizing optical microscopic observations on "heating" process from N* to an isotropic phase in order to avoid a supercooling effect, ii) the Bragg wavelengths in BPs were plotted as a function of temperature to identify phase transitions among different BPs, iii) the temperature ranges showing a coexistence of isotropic phase and BPs were clarified with polarizing optical microscope, then excluded from the temperature range of BPs, with the clearing point T_C defined to be the lowest temperature where the state becomes completely isotropic, and iv) after application and then removal of an electric field, it was confirmed whether BPs were naturally restored from electric field-induced N* at any temperature of BP. If a BP was restored from electric field-induced N* through this procedure, it should be a thermodynamically stable BP at the observed temperature, if not, it should be a metastable BP.

To evaluate the effect of the dendron molecule on the thermodynamically stable BPs, four kinds of samples were prepared (see the Experimental Section). The constituent fractions of samples studied here are shown in **Table 1**. For the measurements of

Table 1. Constituent fractions of samples.

Sample no.	Mixture ratio of host LC [wt%]		CD
	LC mixture	Dendron	
1	100.00	–	–
2	90.00	10.00	–
3	92.50	–	7.50
4	82.50	10.00	7.50

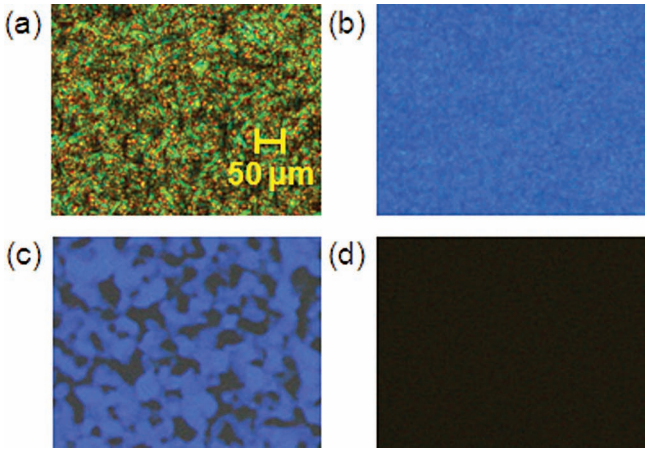

Figure 2. Polarizing optical microscopy images of sample 4: a) focal conic texture of N* at 29.0 °C, b) BP I at 29.9 °C, c) BP II at 30.5 °C, and d) isotropic phase at 35.0 °C.

BP ranges, sample 4 with the dendron molecule was compared with sample 3 without. Samples 1 and 2, which were the host liquid crystals of samples 3 and 4, respectively, were prepared to measure the Frank elastic constants because a method to measure directly the elastic constants of a chiral nematic phase with short helical pitch and blue phase is generally unestablished.

2.1.1. Characterization

BPs are known to show three thermodynamically stable phases, blue phase I (BP I), blue phase II (BP II), and blue phase III (BP III), in order from lower temperature, in a temperature range between a chiral nematic phase and an isotropic phase. **Figure 2** shows polarizing optical microscopy images of the optical textures for sample 4. A typical focal conic texture of N* was observed at lower temperature than 29.2 °C, as shown in Figure 2a. On gradual heating from N*, three phase transitions were observed between the chiral nematic phase and the isotropic phase, probably N*/BP I, BP I/BP II, and BP II/isotropic phase. Figures 2b and c are the optical textures at temperature ranges from 29.3 to 30.4 °C and from 30.5 to 33.9 °C, respectively. The optical textures of BP I and BP II showed no birefringence but were colored, which is the typical nature of BPs. No birefringence without color was observed in the isotropic phase at higher temperatures than 35.0 °C, as shown in Figure 2d.

In the next step, the type of BP for sample 4 was identified from the Bragg diffraction observations. **Figure 3** shows the reflection spectra of sample 4. In N*, a broad peak corresponding to light-scattering of focal conic texture was observed. On heating from N*, sharp peaks appeared at 470 and 411 nm, at 29.9 and 30.5 °C, respectively. It is well-known that the structures of BP I and BP II are body-centered-cubic symmetry and simple-cubic symmetry, respectively, and BP III is seemingly amorphous with local structure.[8,47,48] The ratio among Bragg wavelengths at the lattice planes of body-centered cubic in BP I represents (110):(200):(211):(220) = $1:1/\sqrt{2}:1/\sqrt{3}:1/2$, and (100):(110):(111) = $1:1/\sqrt{2}:1/\sqrt{3}$ for BP II. The relation of Miller index and Bragg wavelength of BP I is expressed as

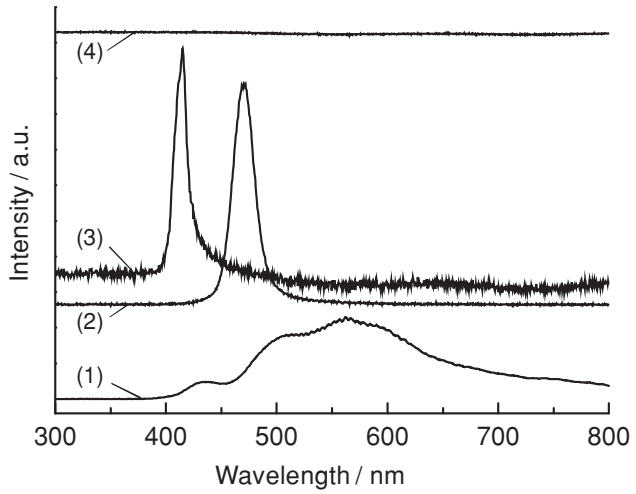

Figure 3. Bragg wavelengths for N*, BP I, BP II, and isotropic phase in sample 4: 1) light scattering of focal conic texture in N* at 29.0 °C, 2) (110) peak of BP I at 29.9 °C, 3) (100) peak of BP II at 30.5 °C, and 4) isotropic phase at 34.2 °C.

$$\lambda = \frac{2na}{\sqrt{h^2 + k^2 + l^2}}$$

where λ, n, and a are the Bragg wavelength, a refractive index and a lattice constant, respectively, and h, k, and l are Miller's indices. Also, since the lattice constant of BP II is half that of BP I, the reflection peak due to the (100) plane of BP II appears generally at a wavelength between the (110) peak and the (200) peak of BP I.[8,47,48] Thus, the Bragg wavelengths at 29.9 and 30.5 °C can be assigned to BP I and BP II, respectively. With rising temperature from BP II, the (100) peak of BP II disappeared at 34.2 °C. This is due to the phase transition from BP II to isotropic phase. For BP III, it is well-known that a broad peak corresponding to a local structure in the reflection spectrum and no boundary optical texture are observed.[35,48] In samples 3 and 4, the characteristics of BP III were not clearly observed between the BP II and the isotropic phase.

After an electric field was applied to the BPs at each temperature and the N* was induced, it was confirmed that the BPs were completely restored from the electric field-induced N* after removing the electric field, as described in detail later in this paper. This behavior observed at any BP temperature is significantly supportive evidence to show the thermodynamic stability of BPs. In a same manner, the phase behavior of sample 3 was investigated. The phase-transition behavior and characterization in sample 3 agreed well with the previous reports.[16,49,50]

2.1.2. Temperature Range of Thermodynamically Stable Liquid Crystalline Blue Phases

The Bragg wavelengths of BPs in a visible wavelength region for samples 3 and 4 were plotted as a function of a relative temperature on the basis of each clearing point T_C, as shown in **Figure 4**. The temperature ranges of BP I and BP II were defined as $\Delta T_{BP\ I} = T_{BP\ I–BP\ II} - T_{N}*_{–BP\ I}$ and $\Delta T_{BP\ II} = T_{BP\ II–(BP+Iso)} - T_{BP\ II\text{-}BP\ I}$. A list of detailed temperature ranges of BPs is shown in **Table 2**. For sample 3 without the dendron molecule, the temperature ranges of BP I and BP II were $\Delta T_{BP\ I} = 0.5$ °C and $\Delta T_{BP\ II} = 1.6$ °C (Figure 4a), respectively. In contrast, for sample 4 including the dendron molecule, they were $\Delta T_{BP\ I} = 1.1$ °C and $\Delta T_{BP\ II} = 3.5$ °C (Figure 4b). Temperature ranges having a coexistence of BP II and isotropic phase (see Figures S1h and i, and S2h and i in the Supporting Information) were excluded from the temperature ranges of BP II in this study. The defining temperature ranges of coexistence as $\Delta T_{BP+Iso} = T_C - T_{BP\ II\text{-}(BP+Iso)}$ were $\Delta T_{BP+Iso} = 0.3$ °C in sample 3 and $\Delta T_{BP+Iso} = 1.1$ °C in sample 4.

The pitch length of helical structure is known to be an important factor affecting the temperature range of BPs. As the pitch of N* becomes shorter from 500 to 150 nm, the temperature ranges of BPs have been reported to increase by 1–2 °C.[51–55] Even when the concentration of the chiral dopant in sample 3 was adjusted so that the helical pitch was consistent with that of sample 4, the temperature range ΔT_{BP} was about 2.1 °C, less than the value of 4.6 °C for sample 4. Therefore, it is concluded clearly that the temperature range of thermodynamically stable BPs was enlarged by doping with the dendron molecule.

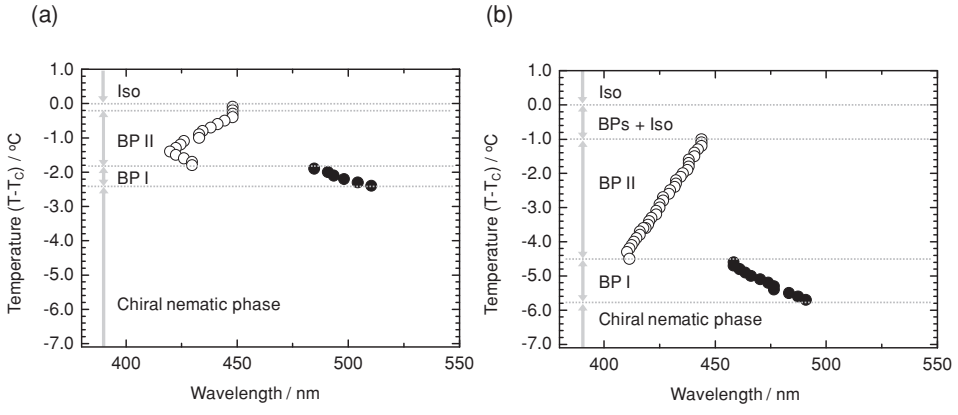

Figure 4. Bragg wavelength of visible range as a function of temperature in BPs: a) sample 3, and b) sample 4. T is the measured temperature, T_C the clearing point. The closed and open circles show the Bragg wavelengths for (110) alignment of BP I and (100) alignment of BP II, respectively.

Table 2. Phase transition temperatures and temperature ranges for samples 3 and 4. The values in brackets indicate the relative temperature on the basis of each clearing point.

Sample no.	Phase - transtion temperature [°C]				Temperature range [°C]		
	N* – BP I	BP I – BP II	BP II – BP II+Iso	BP II+Iso – Iso	$\Delta T_{BP\ I}$	$\Delta T_{BP\ II}$	$\Delta T_{BP\ II+Iso}$
3	42.6 (–2.4)	43.1 (–1.9)	44.7 (–0.3)	45.0 (0.0)	0.5	1.6	0.3
4	29.3 (–5.7)	30.3 (–4.6)	33.9 (–1.1)	35.0 (0.0)	1.0	3.6	1.1

2.1.3. Elastic Properties of Host Nematic Liquid Crystals

BPs are known to be a frustrated phase resulting from the competition between twisting power and packing topology.[55–61] In the free energies of BPs, the three types of the Frank elastic constants, splay (K_{11}), twist (K_{22}), and bend (K_{33}), have been shown theoretically to be closely associated with the thermodynamic stability of BPs. Therefore, in order to consider a possible mechanism of the doping effect on temperature ranges of BPs, we investigated the influence of doping with the dendron molecule on the elastic constants of the host nematic liquid crystal. The temperature dependencies of the elastic constants, K_{11} and K_{33} for samples 1 and 2 are shown in **Figure 5**. It is interesting to note that K_{11} of sample 2 (with dendron molecule) was larger than that of sample 1 (without dendron molecule) as shown in Figure 5a, whereas K_{33} of sample 2 was much smaller than that of sample 1, as shown in Figure 5b. The observed elastic constant ratio, K_{33}/K_{11} of sample 2 is exceedingly small compared to that of typical nematic liquid crystals (Figure 5c).

It is theoretically predicted that the elastic constant ratio K_{33}/K_{11} is associated with an apparent molecular aspect ratio; the ratio of molecular length-to-width, L/D. When the L/D ratio of the molecule is small, K_{33}/K_{11} is expected to become smaller.[62–64] Experimentally, it has been reported that a

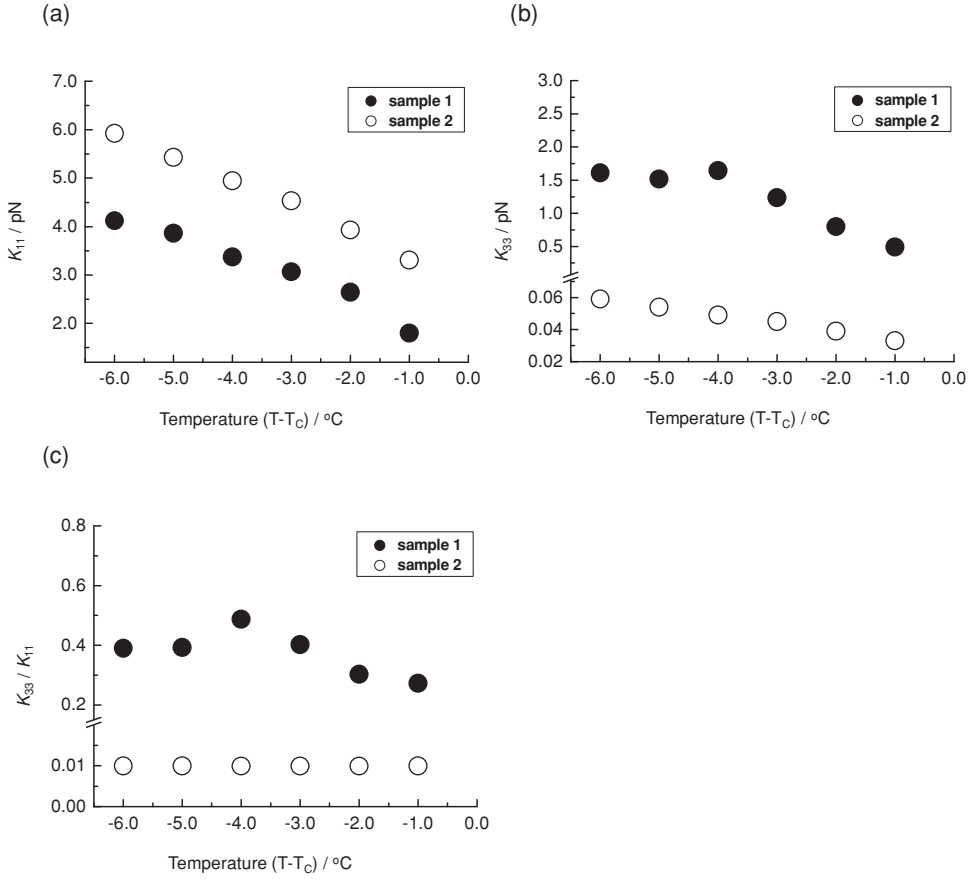

Figure 5. Elastic constants as a function of temperature in nematic phase: a) splay elastic constant (K_{11}), b) bend elastic constant (K_{33}), and c) elastic constant ratio (K_{33}/K_{11}). T is the measured temperature and T_C the clearing point. The closed and open circles show sample 1 (without dendron molecule) and sample 2 (with dendron molecule), respectively.

Table 3. Phase - transition temperature for samples of different dendron concentration.

Mixture ratio of host LC [wt%]			Phase transition temperature [°C]				Temperature range [°C]		
LC mixture	Dendron	CD	BP I	BP II	BP+Iso	Iso	$\Delta T_{BP\ I}$	$\Delta T_{BP\ II}$	ΔT_{BP+Iso}
92.50	–	7.50	42.6	43.1	44.7	45.0	0.5	1.6	0.3
97.50	5.00	7.50	36.7	37.5	39.6	39.9	0.8	2.1	0.3
82.50	10.00	7.50	29.3	30.3	33.9	35.0	1.0	3.6	1.1
77.50	15.00	7.50	22.4	–	26.0	30.0	3.6	–	4.0
72.50	20.00	7.50	12.0	–	14.2	21.0	2.2	–	6.8

side-chain-type liquid crystalline polymer reduced the elastic constant ratio K_{33}/K_{11} of the host nematic liquid crystal down to nearly zero when it was added to the host nematic liquid crystal. This might be due to the apparent decrease in L/D of molecules by smectic-like short-range order.[65] A liquid crystalline dendron molecule has been also shown to have small K_{33} and K_{33}/K_{11} as compared to typical nematics, which might result from the molecular shape and the conformation.[66] Thus, similarly, in the case of the addition of dendron molecule into the host nematic liquid crystals, a decrease in apparent molecular aspect ratio would contribute to the decrease in K_{33}/K_{11}.

The twisting strength of host nematic liquid crystal, which is one factor determing the helical pitch of N*, is known to strongly depend upon K_{22}; this can be shown by a helical twisting power (HTP_{mol}). To estimate the quantity of change in K_{22} due to the dendron molecule doping, the HTP_{mol} of samples 3 and 4 were measured at $T - T_{N^*-BP\ I} = -1.0$ °C; they were 99.0 and 99.2 μm^{-1}, respectively. Therefore the K_{22} of liquid crystal mixture was hardly changed by doping with the dendron molecule.

2.1.4. Free Energy and Elastic Constants

From an energetic perspective, the frustrated structures of BPs are well-known to be divided into two regions of the double twisted cylinder (DTC) and the $s = -1/2$ disclination line,[4,6,8,19,30,55–59,67] The DTC has been theoretically proven to be made up mainly by the deformations of twist (K_{22}) and bend (K_{33}).[55] Also, it has been reported that the DTC favors smaller K_{33}/K_{11} when K_{24} is positive.[68] Common to both, a decrease in K_{33} would reduce the free energy of DTC. Moreover, it has been reported, based on computer calculations and Landau-de Gennes theory, that BPs become unstable when the K_{33} is large or the K_{22} is small as compared to the K = constant approximation.[69] For the $s = -1/2$ disclination line, it has been reported that the stability of BPs with respect to the simple twist of N* is also deeply associated with the elastic constants of K_{11}, K_{22}, K_{33}, and K_{24}.[56] In addition, the association between the elastic constants and the free energy of BPs has been demonstrated with computer calculation.[70–72] No discrepancy is found between the theoretical considerations[55,68–72] and our results; in particular, the theories of DTC[55,68] and computer calculations[72] are in good agreement with our results that the marked decrease in K_{33} enlarged the temperature ranges of BPs. Thus, in our new material system, it is experimentally demonstrated that the decrease in K_{33} should be responsible for the doping-induced enlargement of temperature ranges of thermodynamically stable BPs.

Further, for the disclination line of BPs, it has been reported that an excess energy is needed to create a disclination core with lower-order-parameter-like isotropic liquid at a temperature below the clearing point.[55,56] The order parameter (S), which is used to describe molecular orientational order in liquid crystal, has been also reported to be associated with the L/D ratio.[73] The order parameter decreases when the molecular L/D ratio is reduced. In our results, when the dendron molecule having the small molecular aspect ratio was doped into the host nematic liquid crystal, the order parameter of the doped liquid crystal would be reduced, resulting in lowering of the N*–BPs transition temperature. This is also a possible mechanism of doping-induced enlargement of BPs temperature range.

2.1.5. Dendron Concentration Dependence of the Temperature Range

Next, we investigated the effect of dendron concentration on the BP temperature range. The mixture ratios of five prepared samples and the corresponding phase transition temperatures are shown in **Table 3**. Among the samples including 0, 5, and 10 wt% of dendron molecules, the BP temperature range was enlarged with increasing dendron molecule content. In contrast, not only the BP range but also the coexistence range of a BP and an isotropic phase was enlarged in the samples including more than 10 wt% of the dendron molecules. The enlargement of the range of coexistence may be caused by the poor solubility of dendron molecules in the liquid crystalline phase.

2.2. Electro-Optical Properties of Liquid Crystalline Blue Phases

2.2.1. Continuous Shift of Bragg Wavelength

Figure 6a,b show the electric field dependency of Bragg wavelengths for the BPs of samples 3 and 4. The closed and open circles in Figure 6 show the results for BP I and BP II, respectively. Interestingly, in both samples 3 and 4, the Bragg wavelengths of BP I continuously shifted to longer wavelength (red-shift) with increasing voltage, whereas discontinuous jumps of Bragg wavelengths of BP II were observed in addition to the continuous red-shifts.

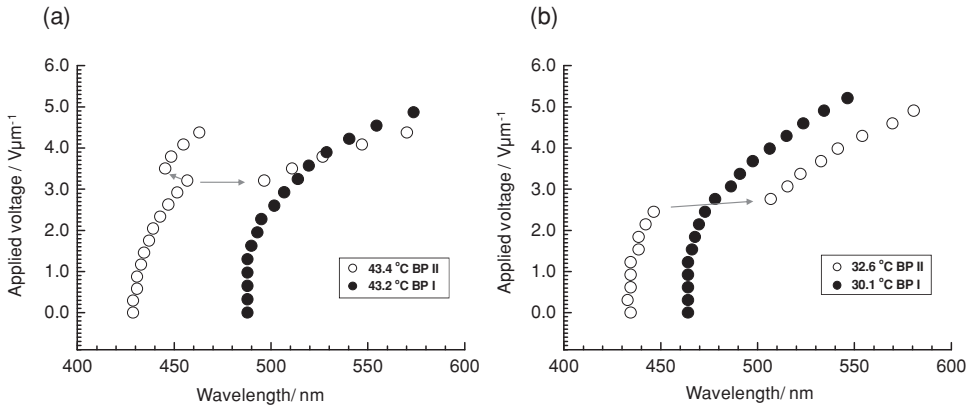

Figure 6. Bragg wavelengths as a function of applied voltage in BPs: a) sample 3 and b) sample 4. The closed and open circles at 0 V μm^{-1} show the Bragg wavelengths for (110) alignment of BP I and (100) alignment of BP II, respectively. The arrow shows a jump of Bragg wavelength.

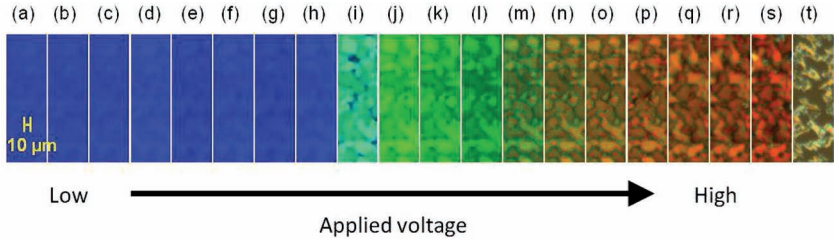

Figure 7. Color switching and electric field-induced phase transition on polarizing optical microscopy images as a function of applied field in sample 4 at 32.6 °C ($T - T_C = -2.4$ °C): a-h) BP II, i-s) BP X, and t) N*. Conditions:a) 0, b) 0.41, c) 0.81, d) 1.23, e) 1.64, f) 2.05, g) 2.46, h) 2.87, i) 3.28, j) 3.69, k) 4.10, l) 4.51,m) 4.79, n) 4.88, o) 4.92, p) 4.97, q) 4.99, r) 5.02, s) 5.08, and t) 5.25 V μm^{-1}.

It is known that the continuous shifts and the jumps for Bragg wavelengths correspond to the continuous deformation of cubic lattice and the phase transitions upon an electric field in BPs, respectively.[6,74–87] Especially, the relation between the jumps of Bragg wavelengths and the electric field-induced phase transitions of BP II–BPX and BP X–3D hexagonal symmetry blue phase (BP H^{3D}) has been demonstrated with a Kossel diagram.[77–79] Our results are in good accordance with the results obtained by Pierański et al.[77] and Chen et al.[81] Consequently, the jumps of Bragg wavelengths in BP II on the electric field observed in our study might be electric field-induced phase transitions from BP II to BP X and BP H^{3D}.

Figure 7 shows the electric field dependence of polarizing optical microscopy images for the BP II of sample 4 at $T - T_C = -2.4$ °C. As the applied voltage was increased, the various colors switching of blue, green, and red corresponding to a continuous shift of Bragg wavelength under the electric field were observed. The color switching times from green to red have been experimentally proven to be of millisecond order.[34,88] The shift ranges and the switching times for BPs were comparable to those of polymer-stabilized N* systems.[89,90]

2.2.2. Temperature Dependence of Shift Range of Bragg Wavelength

In order to evaluate the electro-optical properties of BPs toward practical device applications, the relation between the temperature and the shift ranges of Bragg wavelengths of BPs on the electric field, which was defined as a difference between initial wavelength and maximally shifted wavelength ($\Delta\lambda = \lambda_{initial} - \lambda_{max}$), was investigated; the results are shown in **Figure 8**. At the lowest temperature of BP I, the shift ranges of samples 3 and 4 were from 510 to 534 nm ($\Delta\lambda$ = 24 nm) and from 487 to 516 nm ($\Delta\lambda$ = 29 nm), respectively. In contrast, at the highest temperature they were from 483 to 557 nm ($\Delta\lambda$ = 74 nm) and from 463 to 572 nm ($\Delta\lambda$ = 109 nm). The shift ranges of BP I gradually expanded with rising temperature in both samples 3 and 4.

The deformation behavior of BP lattices under electric fields resulting from a competition between elastic force and electric force has been theoretically reported; it is described as a difference of free-energy change (ΔF_{BP}) between an initial state (F_0) and an excited state at a critical point of electric field-induced BP–N* transition (F_{BP-N}*).[91–98] However, the correlation between the temperature change and the shift range in BPs has never been discussed. Therefore, we focused on the critical electric field of the electric field-induced BP–N* transitions in order to investigate the correlation. It is well known that electric field-induced phase transitions of BP–N* and N*–nematic phase (N) occur in order with increasing voltage when an electric field is applied to BPs.[5] In particular, the critical electric field of electric field-induced N*–N transition, which reflects the stability of N* against N under the electric field, has been theoretically shown to depend upon the dielectric anisotropy, the helical pitch, and the elastic constant.[55] The dielectric anisotropy and the elastic constant would be also major physical parameters to determine the stability of BPs against N*. To experimentally estimate the phase stability of BP I with respect to electric force, a critical electric field of electric field-induced BP I–N* transition ($E_{BP\ I-N}$*) was plotted as a function of a relative temperature from each $T_{BP\ I-BP\ II}$, as shown in **Figure 9**. At the lowest temperature of BP I, the critical electric fields of samples 3 and 4 were 3.2 and 3.4 V μm^{-1}, respectively. In contrast, at the highest temperature they were 4.7 and 5.8 V μm^{-1}. The critical electric field

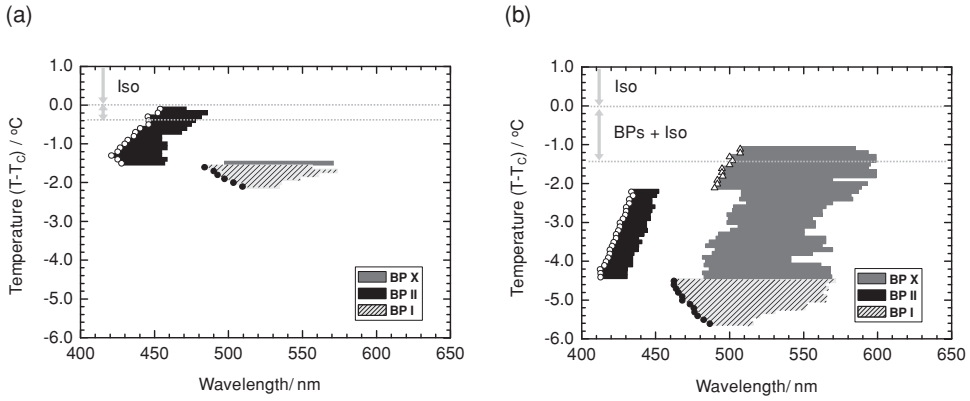

Figure 8. Temperature dependency of the electric field-induced reversible shifts of Bragg wavelength for BPs: a) sample 3 and b) sample 4. T is the measured temperature and T_C is the clearing point. The closed circles, open circles, and open triangles show the Bragg wavelengths of BPs after removing the electric-field. The diagonal regions of light gray, black, and dark gray show the electric field-induced reversible shift ranges of Bragg wavelengths of BP I, BP II, and BP X, respectively.

also clearly increased with rising temperature in addition to the shift ranges of BP I. This result indicates that the stability of BP I with respect to N* is gradually enhanced with rising temperature.

The BP X temperature ranges of samples 3 and 4 ($\Delta T_{BP\ X}$) were 0.1 and 2.9 °C, respectively, as shown in Figures 8a and b; the range was clearly enlarged by the dendron molecule doping. For the temperature ranges $T - T_C = -1.5$ °C and −0.4 °C in sample 3, the electric field-induced phase transition from BP II to not BP X but an uncharacterized phase was observed. The uncharacterized phase, which was very dark with bluish coloring on polarized optical microscopic observation, showed no Bragg wavelength of visible region. A similar phase, which showed no Bragg wavelength of visible region, has been reported to be characterized as a 2D hexagonal symmetry blue phase (BP H^{2D}).[86,87] Accordingly, the uncharacterized phase in our result might be BP H^{2D}. For the temperature range $T - T_C = -2.1$ and −1.4 °C in sample 4, the original state was not restored from the electric field-induced N*, and BP X remained unchanged after the removal of the electric field. As described above, it is known that the major parameters to determine the stability of BPs on the electric field are the elastic constant and the dielectric anisotropy. In case of the liquid crystal mixture doped with dendron molecules, the change in the elastic constants was large and the changes in the dielectric anisotropy and the helical pitch of N* were small. Therefore, the change in elastic constants may be one of the reasons that the stability of BP X is enhanced.

3. Conclusions

We successfully enlarged the temperature ranges of thermodynamically stable BP I, BP II, and BP X by doping with the

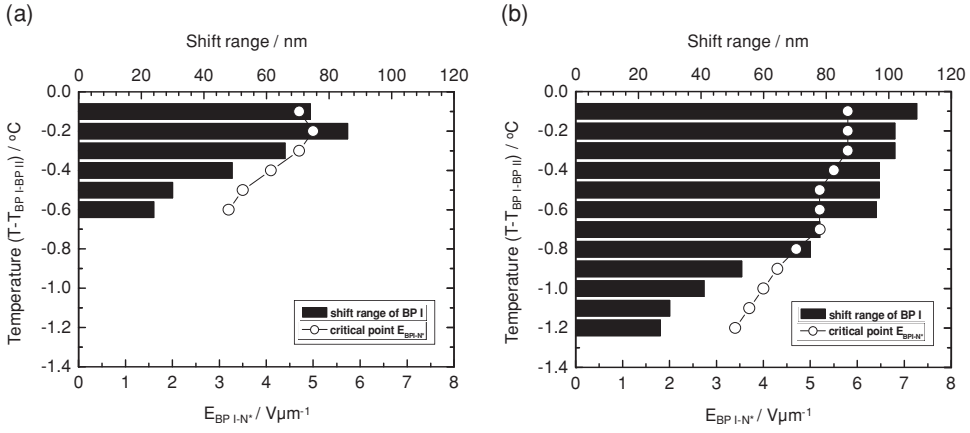

Figure 9. Temperature versus electric field-induced reversible shift of Bragg wavelength for BP I and critical electric field ($E_{BP\ I–N}$*): a) sample 3 and b) sample 4. The crossbars and the open circles show the electric field-induced reversible shift range of Bragg wavelength of BP I and the critical electric field of electric field-induced BP I–N* transition, respectively. The zero on the temperature axis shows the phase transition temperature from BP I to BP II ($T_{BP\ I–BP\ II} = 0.0$ °C).

dendron molecule. Over the whole temperature ranges of BPs, the thermodynamically stable states were experimentally demonstrated from the phenomenon that a chiral nematic phase induce by an electric field was restored to BP after removing the electric field. Furthermore, it was found that the critical electric fields of the electric field-induced phase transitions from BP I and BP X to N* were increased by the dendron-molecule doping, which leads to the wide shift ranges of Bragg wavelength. The possible mechanism of these results may be due to a change in elastic constants of the host liquid crystal and the decrease in orientational order of the molecules.

4. Experimental Section

As a host nematic liquid crystal (host LC), a mixture of fluorinated nematic liquid crystals (JC1041-XX, JNC Co., Δn = 0.142, $\Delta\varepsilon$ = 5.7 at 25 °C)/4-cyano-4′-pentyl biphenyl (5CB, Aldrich, Δn = 0.19, $\Delta\varepsilon$ = 11 at 25 °C) = 1:1 were used.[8–16,49,50] A dendron molecule was newly synthesized to enlarge the BP temperature range. The chemical structure of the dendron molecule is shown in Figure 1 (see also Scheme S1,S2 in the Supporting Information). A chiral dopant (CD), 2,5-bis-[4′-(hexyloxy)-phenyl-4-carbonyl]-1,4;3,6-dianhydride-D-sorbitol (ISO(6OBA)$_2$) was mixed with the host LC to induce BPs.[11–16,49,50] The chemical structures of JC1041-XX, 5CB and ISO(6OBA)$_2$ are shown in Figure S3 in the Supporting Information.

For measurements of temperature-dependency of Bragg wavelengths in BPs, an ITO-coated glass-sandwiched cell by which an electric field can be applied in a direction perpendicular to a substrate surface was used (E. H. C. Co.). The cell gap was about 15 µm, which was determined from optical interference with a UV-Vis spectrophotometer (JASCO, MSV-350). The optical textures of samples were observed under the crossed Nicols with a polarizing optical microscope (POM; Leica, DMLP LP-3). The Bragg wavelengths of BPs were measured with a polarizing optical microscope (Nikon, ECLIPSE E600 PDL) equipped with a multichannel spectroscopic-photometer (Hamamatsu Photonics, PMA-11). The temperatures of the samples were precisely controlled by a hot stage (Linkam, LTS-E350), in which the temperature can be controlled by a temperature controller (Linkam, 10013L) with an accuracy of ±0.1 °C.

For the temperature dependency of electric field–induced reversible shifts of Bragg wavelengths of visible region in BPs, the measuring operations were repeated as follows: i) the Bragg wavelengths were measured from 0 to 100 V in 5 V steps of an a.c. electric voltage at 1 kHz, ii) a critical electric voltage of field-induced BP-N* transition was confirmed with increasing voltage, iii) the original state was naturally restored after removal of the electric field, and iv) the temperature of the sample was increased by 0.1 °C.

To measure a helical pitch of N*, a wedge cell, of which the inner surfaces were coated with polyimide thin film and rubbed in parallel to give a homogeneous liquid crystal alignment, was used (tanθ = 0.079 ° ± 10%) (E. H. C. Co.). A helical twisting power (HTP$_{mol}$) was derived from the following equation.

$$\mathrm{HTP}_{mol} = 1/pc$$

where p is the helical pitch of N* and c is the molar concentration of chiral dopant.

For the measurement of elastic constants, each sample was filled into a glass-sandwiched cell with ITO circle electrode of 1 cm^2. The cell gap, d was adjusted to 18.8 µm by film spacers. A poly(vinyl alcohol) thin film was coated on the glass substrates as a homogeneous alignment layer. The rubbing directions of upper and lower substrates were antiparallel. The electric fields were applied in the direction perpendicular to the substrate surface. For the applied electric field to measure voltage dependency of the electric capacitance, a small sine-wave a.c. field with 1 kHz frequency was imposed to a square-wave a.c. field with 10 Hz frequency. The electric capacitance was evaluated by the small sine-wave of a.c. field at 1 kHz, and the nematic director was reoriented by the square-wave of a.c. field at 10 Hz. The applied voltage of square-wave of a.c. field at 10 Hz was increased in 0.1 V steps from 0 to 15 V. A threshold voltage (V_{th}) and a dielectric constant anisotropy ($\Delta\varepsilon$) were determined with capacitance method using a capacitance–voltage (C–V) measurement system (Toyo Co.). The elastic constant of K_{11} was derived from the following equation

$$V_{th} = \pi\sqrt{\frac{K_{11}}{\varepsilon_0|\Delta\varepsilon|}}$$

where ε_0 is vacuum permittivity. The C–V curves were fitted to the equation to approximate the elastic constants K_{33}

$$\frac{C}{C_0} = \frac{2}{\pi}\sqrt{1+\gamma\sin^2\theta_m}\ \frac{V_{th}}{V}\ \int_0^{\theta_m}\sqrt{\frac{\left(1+\gamma\sin^2\theta\right)\left(1+\kappa\sin^2\theta\right)}{\sin^2\theta_m+\sin^2\theta}}\,d\theta$$

$$\kappa = \frac{K_{33}-K_{11}}{K_{11}}$$

$$\gamma = \frac{\varepsilon_{\parallel}-\varepsilon_{\perp}}{\varepsilon_{\parallel}}$$

where C_0 is the initial capacitance, γ the normalized dielectric constant, κ the elastic constant ratio, and θ the tilt angle at $d/2$ depth. The fitting of C–V curves was performed by matching the fitting parameter chi-square distribution for samples 1 and 2, as shown in **Tables 4** and **5**.

Table 4. Temperature dependency of elastic constants in sample 1; K_{11} and K_{33}, elastic constant ratio; K_{33}/K_{11}, dielectric constant anisotropy; $\Delta\varepsilon$, threshold voltage; V_{th}, fitting parameters; γ and κ, chi-square distribution; chi^2.

JC1041-XX/5CB(sample 1)								
T–T_C(°C)	$\Delta\varepsilon$	V_{th} [V]	Y	k	chi^2	K_{11}(pN)	K_{33}(pN)	K_{33}/K_{11}
–1.0	4.128	0.698	0.631	–0.727	1041 E–0.5	1.80	0.49	0.27
–2.0	5.049	0.764	0.814	–0.698	2.92 E–0.5	2.64	0.80	0.30
–3.0	5.575	0.783	0.919	–0.598	4.24 E–0.5	3.07	1.23	0.40
–4.0	6.019	0.791	1.013	–0.480	4.45 E–0.5	3.38	1.76	0.52
–5.0	6.269	0.826	1.067	–0.580	4.66 E–0.5	3.84	1.61	0.42
–6.0	6.568	0.842	1.138	–0.600	6.87 E–0.5	4.18	1.67	0.40

Table 5. Temperature dependency of elastic constants in sample 2; K_{11} and K_{33}, elastic constant ratio; K_{33}/K_{11}, dielectric constant anisotropy; $\Delta\varepsilon$, threshold voltage; V_{th}, fitting parameters; γ and κ, chi-square distribution; chi^2.

JC1041-XX/5CB/dendron (sample 2)								
$T-T_C$(°C)	$\Delta\varepsilon$	V_{th} [V]	Y	k	chi^2	K_{11}(pN)	K_{33}(pN)	K_{33}/K_{11}
–1.0	4.279	0.849	0.654	–0.990	5.45 E–05	2.765	0.028	0.010
–2.0	5.096	0.883	0.796	–0.990	5.47 E–05	3.565	0.037	0.010
–3.0	5.490	0.928	0.890	–0.990	3.28 E–05	4.239	0.042	0.010
–4.0	5.862	0.950	0.967	–0.990	3.23 E–05	4.747	0.047	0.010
–5.0	6.122	0.968	1.032	–0.990	4.03 E–05	5.146	0.051	0.010
–6.0	6.425	0.985	1.098	–0.990	3.96 E–05	5.595	0.056	0.010

Supporting Information

Supporting Information is available from the Wiley Online Library or from the author.

Acknowledgements

This work was partially supported by a Grant-in-Aid for Scientific Research (A) of the Japan Society for the Promotion of Science (JSPS), a Grant-in-Aid for Scientific Research on Innovative Areas of "Fusion Materials: Creative Development of Materials and Exploration of Their Function through Molecular Control" (no. 2206) and the Global COE Program for "Novel Carbon Resource Sciences; Coal-Based Eco-Innovations" from the Ministry of Education, Culture, Sports, Science and Technology, Japan (MEXT). The authors thank Shin-ichi Yamamoto, Dr. Kosuke Kaneko, Dr. Thet Naing Oo, and Dr. Yukiko Ogawa for helpful discussions.

Received: August 31, 2012
Revised: October 30, 2012
Published online: December 27, 2012

[1] E. Yablonovitch, *Phys. Rev. Lett.* **1987**, *58*, 2059.
[2] J. S. Foresi, P. R. Villeneuve, J. Ferrera, E. R. Thoen, G. Steinmeyer, S. Fan, J. D. Joannopoulos, L. C. Kimerling, H. I. Smith, E. P. Ippen, *Nature* **1997**, *390*, 143.
[3] O. Painter, R. K. Lee, A. Scherer, A. Yariv, J. D. O'Brien, P. D. Dapkus, I. Kim, *Science* **1999**, *284*, 1819.
[4] D. C. Wright, N. D. Mermin, *Rev. Mod. Phys.* **1989**, *61*, 385.
[5] P. P. Crooker, in *Chirality in Liquid Crystals*, (Eds: H.-S. Kitzerow, C. Bahr) Springer, New York **2001**, Ch.7.
[6] H.-S. Kitzerow, *Mol. Cryst. Liq. Cryst.* **1991**, *202*, 51.
[7] P. Etchegoin, *Phys. Rev. E* **2000**, *62*, 1435.
[8] H. Kikuchi, M. Yokota, Y. Hisakado, H. Yang, T. Kajiyama, *Nat. Mater.* **2002**, *1*, 64.
[9] Y. Hisakado, H. Kikuchi, T. Nagamura, T. Kajiyama, *Adv. Mater.* **2005**, *17*, 96.
[10] H. Kikuchi, S. Hirata, K. Uchida, *Mol. Cryst. Liq. Cryst.* **2007**, *465*, 283.
[11] Y. Haseba, H. Kikuchi, *Mol. Cryst. Liq. Cryst.* **2007**, *470*, 1.
[12] T. Iwata, T. Tanaka, K. Suzuki, N. Amaya, H. Higuchi, H. Kikuchi, *Mol. Cryst. Liq. Cryst.* **2007**, *470*, 11.
[13] K. Higashiguchi, K. Yasui, H. Kikuchi, *J. Am. Chem. Soc.* **2008**, *130*, 6326.
[14] H. Kikuchi, in *Liquid Crystalline Functional Assembles and their Supramolecular Structures* (Eds: T. Kato, D. M. P. Mingos), Springer, Berlin **2008**, p. 99–117.
[15] T. Iwata, K. Suzuki, N. Amaya, H. Higuchi, H Masunaga, S. Sasaki, H. Kikuchi, *Macromolecules* **2009**, *42*, 2002.
[16] T. Iwata, K. Suzuki, H. Higuchi, H. Kikuchi, *Liq. Cryst.* **2009**, *36*, 947.
[17] J. Yan, M. Jiao, L. Rao, S. T. Wu, *Opt. Express* **2010**, *18*, 11450.
[18] J. Yan, H. C. Cheng, S. Gauza, Y. Li, M. Jiao, L. Rao, S. T. Wu, *Appl. Phys. Lett.* **2010**, *96*, 071105.
[19] J. Fukuda, *Phys. Rev. E* **2010**, *82*, 061702.
[20] L. Rao, J. Yan, S. T. Wu, S.-I. Yamamoto, Y. Haseba, *Appl. Phys. Lett.* **2011**, *98*, 081109.
[21] J. Yan, Y. Li, S. T. Wu, *Opt. Lett.* **2011**, *36*, 1404.
[22] T. N. Oo, T. Mizunuma, Y. Nagano, H. Ma, Y. Ogawa, Y. Haseba, H. Higuchi, Y. Okumura, H. Kikuchi, *Opt. Mater. Express* **2011**, *1*, 1502.
[23] T. Mizunuma, T. N. Oo, Y. Nagano, H. Ma, Y. Haseba, H. Higuchi, Y. Okumura, H. Kikuchi, *Opt. Mater. Express* **2011**, *1*, 1561.
[24] L. Wang, W. He, X. Xiao, F. Meng, Y. Zhang, P. Yang, L. Wang, J. Xiao, H. Yang, Y. Lu, *Small* **2012**, *8*, 2189.
[25] W. Cao, A. Muñoz, P. Palffy-Muhoray, B. Taheri, *Nat. Mater.* **2002**, *1*, 111.
[26] S. Yokoyama, S. Mashiko, H. Kikuchi, K. Uchida, T. Nagamura, *Adv. Mater.* **2006**, *18*, 48.
[27] J. Schmidtke, W. Stille, H. Finkelman, *Phys. Rev. Lett.* **2003**, *90*, 083902.
[28] M. H. Song, B. Park, K. Shin, T. Ohta, Y. Tsunoda, H. Hoshi, Y. Takanishi, K. Ishikawa, J. Watanabe, S. Nishimura, T. Toyooka, Z. Zhu, T. M. Swager, H. Takezoe, *Adv. Mater.* **2004**, *16*, 779.
[29] Y. Matsuhisa, R. Ozaki, M. Ozaki, K. Yoshino, *Jpn. J. Appl. Phys.* **2005**, *44*, L629.
[30] H. Yoshida, Y. Tanaka, K. Kawamoto, H. Kubo, T. Tsuda, A. Fujii, S. Kuwabata, H. Kikuchi, M. Ozaki, *Appl. Phys. Express* **2009**, *2*, 121501.
[31] H. Yoshida, K. Kawamoto, H. Kubo, T. Tsuda, A. Fujii, S. Kuwabata, M. Ozaki, *Adv. Mater.* **2010**, *22*, 622.
[32] M. Ravnik, G. P. Alexander, J. M. Yeomans, S. Žumer, *Proc. Natl. Acad. Sci. USA* **2011**, *108*, 5188.
[33] M. Nakata, Y. Takanishi, J. Watanabe, H. Takezoe, *Phys. Rev. E* **2003**, *68*, 041710.
[34] H. J. Coles, M. N. Pivnenko, *Nature* **2005**, *436*, 997.
[35] M. Sato, A. Yoshizawa, *Adv. Mater.* **2007**, *19*, 4145.
[36] W. He, G. Pan, Z. Yan, D. Zhao, G. Niu, W. Huang, X. Yuan, J. Guo, H. Cao, H. Yang, *Adv. Mater.* **2009**, *21*, 2050.
[37] A. Yoshizawa, Y. Kogawa, K. Kobayashi, Y. Takanishi, J. Yamamoto, *J. Mater. Chem.* **2009**, *19*, 5759.
[38] S. Taushanoff, K. V. Le, J. Williams, R. J. Twieg, B. K. Sadashiva, H. Takezoe, A. Jakli, *J. Mater. Chem.* **2010**, *20*, 5893.
[39] M. Lee, S. T. Hur, H. Higuchi, K. Song, S.-W. Choi, H. Kikuchi, *J. Mater. Chem.* **2010**, *20*, 5813.

[40] S.-Y. Lu, L.-C. Chien, *Opt. Lett.* **2010**, *35*, 562.
[41] E. Karatairi, B. Rožić, Z. Kutnjak, V. Tzitzios, G. Nounesis, G. Cordoyiannis, C. Glorieux, J. Thoen, S. Kralj, *Phys. Rev. E* **2010**, *81*, 041703.
[42] G. Cordoyiannis, P. Losada-Pérez, C. S. P. Tripathi, B. Rožič, U. Tkalec, V. Tzitzios, E. Karatairi, G. Nounesis, Z. Kutnjak, I. Muševič, C. Glorieux, S. Kralj, J. Thoen, *Liq. Cryst.* **2010**, *37*, 1419.
[43] B. Rožič, V. Tzitzios, E. Karatairi, U. Tkalec, G. Nounesis, Z. Kutnjak, G. Cordoyiannis, R. Rosso, E. G. Virga, I. Muševič, S. Kralj, *Eur. Phys. J. E* **2011**, *34*, 11057.
[44] S.-T. Hur, M.-J. Gim, H.-J. Yoo, S.-W. Choi, H. Takezoe, *Soft Matter* **2011**, *7*, 8800.
[45] J.-M. Wong, J.-Y. Hwang, L.-C. Chien, *Soft Matter* **2011**, *7*, 7956.
[46] L. Wang, W. He, X. Xiao, Q. Yang, B. Li, P. Yang, H. Yang, *J. Mater. Chem.* **2012**, *22* 2383.
[47] D. L. Johnson, J. H. Flack, P. P. Crooker, *Phys. Rev. Lett.* **1980**, *45*, 641.
[48] E. I. Demikhov, V. K. Dolganov, S. P. Krylova, *JETP Lett.* **1985**, *42*, 16.
[49] H. Choi, H. Higuchi, H. Kikuchi, *Soft Matter* **2011**, *7*, 4252.
[50] H. Choi, H. Higuchi, H. Kikuchi, *Appl. Phys. Lett.* **2011**, *98*, 131905.
[51] K. Tanimoto, P. P. Crooker, G. C. Koch, *Phys. Rev. A* **1985**, *32*, 1893.
[52] M. B. Atkinson, P. J. Collings, *Mol. Cryst. Liq. Cryst.* **1986**, *136*, 141.
[53] J. D. Miller, P. R. Battle, P. J. Collings, D.-K. Yang, P. P. Crooker, *Phys. Rev. A* **1987**, *35*, 3959.
[54] D.-K. Yang, P. P. Crooker, *Phys. Rev. A* **1987**, *35*, 4419.
[55] P. G. De Gennes, J. Prost, *The Physics of Liquid Crystals*, 2nd ed, Oxford University Press, Oxford, UK **1993**, Ch. 6.
[56] S. Meiboom, J. P. Sethna, P. W. Anderson, W. F. Brinkman, *Phys. Rev. Lett.* **1981**, *46*, 1216.
[57] J. P. Sethna, D. C. Wright, N. D. Mermin, *Phys. Rev. Lett.* **1983**, *51*, 467.
[58] J. P. Sethna, *Phys. Rev. Lett.* **1983**, *51*, 2198.
[59] J. P. Sethna, in *Theory and Application of Liquid Crystals*, (Eds: J. L. Ericksen, D. Kinderlehrer), Springer-Verlag, New York **1987**, 305.
[60] M. Kléman, *J. Phys. Lett.* **1985**, *46*, L-723.
[61] O. D. Lavrentovich, M. Kléman, in *Chirality in Liquid Crystals* (Eds: H.-S. Kitzerow, C. Bahr) Springer, New York **2001**, Ch. 7.
[62] B. W. Van Der Meer, F. Posma, A. J. Dekker, W. H. De Jeu, *Mol. Phys.* **1982**, *45*, 1227.
[63] M. J. Bradshaw, E. P. Raynes, I. Fedark, A. J. Leadbetter, *J. Phys.* **1984**, *45*, 157.
[64] D. Dunmur, K. Toriyama, in *Handbook of Liquid Crystals*, (Eds: D. Demus, J. Goodby, G. W. Gray, H.-W. Spiess) Wiley-VCH, Weinheim, Germany **1998**, Ch. 7.
[65] S. Kibe, H. Kikuchi, T. Kajiyama, *Liq. Cryst.* **1996**, *21*, 807.
[66] A. J. Jim, M. R. Fisch, M. P. Mahajan, K. A. Crandall, P. Chu, C.-Y. Huang, V. Percec, R. G. Petschek, C. Rosenblatt, *Eur. Phys. J. B* **1998**, *5*, 251.
[67] J. Fukuda, S. Žumer, *Phys. Rev. Lett.* **2010**, *104*, 017801.
[68] M. Kléman, *J. Phys.* **1985**, *46*, 1193.
[69] G. P. Alexander, J. M. Yeomans, *Phys. Rev. E* **2006**, *74*, 061706.
[70] S. Meiboom, M. Sammon, W. F. Brinkman, *Phys. Rev. A* **1983**, *27*, 438.
[71] S. Meiboom, M. Sammon, D. W. Berreman, *Phys. Rev. A* **1983**, *28*, 3553.
[72] J. Fukuda, *Phys. Rev. E* **2012**, *85* 020701.
[73] H. Kimura, *J. Phys. Soc. Jpn.* **1974**, *36*, 1280.
[74] G. Heppke, M. Krumrey, F. Oestreicher, *Mol. Cryst. Liq. Cryst.* **1983**, *99*, 99.
[75] H. Stegemeyer, F. Porsch, *Phys. Rev. A* **1984**, *30*, 3369.
[76] G. Heppke, H.-S. Kitzerow, M. Krumrey, *Mol. Cryst. Liq. Cryst. Lett.* **1985**, *1*, 117.
[77] P. Pierański, P. E. Cladis, R. Barbet-Massim, *J. Phys. Lett.* **1985**, *46*, L-973.
[78] P. E. Cladis, T. Garel, P. Pierański, *Phys. Rev. Lett.* **1986**, *57*, 2841.
[79] P. Pierański, P. E. Cladis, *Phys. Rev. A* **1987**, *35*, 355.
[80] H. Porsch, H. Stegemeyer, *Liq. Cryst.* **1987**, *2*, 395.
[81] N.-R. Chen, J. T. Ho, *Phys. Rev. A* **1987**, *35*, 4886.
[82] M. Jorand, P. Pierański, *J. Phys.* **1987**, *48*, 1197.
[83] G. Heppke, B. Jérôme, H.-S. Kitzerow, P. Pierański, *J. Phys.* **1989**, *50*, 549.
[84] G. Heppke, B. Jérôme, H.-S. Kitzerow, P. Pierański, *J. Phys.* **1989**, *50*, 2991.
[85] G. Heppke, B. Jérôme, H.-S. Kitzerow, P. Pierański, *Liq. Cryst.* **1989**, *5*, 813.
[86] H. Porsch, H. Stegemeyer, *Liq. Cryst.* **1989**, *5*, 791.
[87] B. Jérôme, P. Pierański, *Liq. Cryst.* **1989**, *5*, 799.
[88] H.-Y. Chen, J.-Y. Chiou, K.-X. Yang, *Appl. Phys. Lett.* **2011**, *99*, 181119.
[89] H. Xianyu, T.-H. Lin, S.-T. Wu, *Appl. Phys. Lett.* **2006**, *89*, 091124.
[90] S.-Y. Lu, L.-C. Chien, *Appl. Phys. Lett.* **2007**, *91*, 131119.
[91] R. M. Hornreich, M. Kugler, S. Shtrikman, *Phys. Rev. Lett.* **1985**, *54*, 2099.
[92] D. Lubin, R. M. Hornreich, *Phys. Rev. A* **1987**, *36*, 849.
[93] D. E. Dmitrienko, *Liq. Cryst.* **1989**, *5*, 847.
[94] H. Stark, H.-R. Trebin, *Phys. Rev. A* **1991**, *44*, 2752.
[95] L. Longa, M. Żelazna, H.-R. Trebin, J. Mościcki, *Phys. Rev. E* **1996**, *53*, 6067.
[96] M. Żelazna, L. Longa, H.-R. Trebin, H. Stark, *Phys. Rev. E* **1998**, *57*, 6711.
[97] G. P. Alexander, D. Marenduzzo, *EPL* **2008**, *81*, 66004.
[98] J. Fukuda, M. Yoneya, H. Yokoyama, *Phys. Rev. E* **2009**, *80*, 031706.